Seismic structures of the 154–160 Ma oceanic crust and uppermost mantle in the Northwest Pacific Basin

Mitsuhiro Oikawa, Kentaro Kaneda, and Azusa Nishizawa

Hydrographic and Oceanographic Department, Japan Coast Guard, Tokyo 104-0045, Japan

(Received October 2, 2009; Revised February 21, 2010; Accepted February 25, 2010; Online published April 12, 2010)

We present detailed P-wave velocity models for the Northwest Pacific Basin which were produced in 154–160 Ma at a high seafloor spreading half-rate of >8 cm/yr and have not been appreciably deformed by tectonic or igneous activity since then. We carried out wide-angle seismic experiments on two crossing survey lines which are respectively parallel and perpendicular to paleomagnetic lineations. The seismic crustal models for both lines are almost identical and homogeneous along these lines. The crust consists of an upper layer (Layer 2) with a P-wave velocity V_p = 2.5–6.8 km/s and a thickness of 1.3–2.2 km, and a lower layer (Layer 3) with a velocity of 6.8–7.1 km/s and a thickness of 4.6–5.9 km. These characteristics indicate that the crust beneath the survey line has a standard oceanic crustal structure. The structure of the uppermost mantle of the line parallel to the seafloor spreading direction exhibits considerable V_p heterogeneity within 5 km immediately below the Moho and shows an unusually high V_p of 8.5–8.7 km/s. The P_n velocity for the perpendicular line is 7.9 km/s, and the magnitude of the velocity anisotropy for the uppermost mantle amounts to a large value of 7–10%.

Key words: Oceanic crust, Northwest Pacific Basin, seismic structure, ocean bottom seismograph, anisotropy.

1. Introduction

Oceanic crusts created at mid-ocean ridges are considered to have similar basic structure everywhere, with the exception of anomalous regions such as fracture zones and hotspots (White *et al*., 1992). Most of the structural models of normal oceanic crust were obtained through seismic studies conducted between 1960 and 1980 (e.g., Shor *et al*., 1970; Christensen and Salisbury, 1975). Recently, the remarkable advancement of technologies for studying seismic refraction and reflection (e.g., GPS navigation systems, Ocean Bottom Seismographs (OBS), analytical methods, calculation performance of computers) has allowed for the acquisition of more precise velocity structures (e.g., Kasahara *et al*., 2007; Oshida *et al*., 2008). However, there have been only few seismic explorations aimed at studying normal oceanic crust with the latest technologies.

The area northwest of Minami-Tori Shima Island in the Northwest Pacific Basin is one of the most intriguing areas for investigating typical oceanic crustal structures (Fig. 1). Paleogene magnetic isochron maps (Nakanishi *et al*., 1989, 1992) indicate that the area has formed during as early as the Jurassic period and as late as the Cretaceous period, and it is considered that the area has not been appreciably deformed by tectonic or igneous activity after its formation since clear paleomagnetic lineations can be observed there. The fact that bathymetric fabric is present in the direction perpendicular to the seafloor spreading direction on the ocean floor also supports the theory of little modification of the oceanic crust. This field retains an original crustal structure formed at the mid-ocean ridge.

Accordingly, we carried out two wide-angle seismic experiments on the two survey lines in the area, which were designed to obtain accurate and updated models of the typical oceanic crust and uppermost mantle (Fig. 1).

2. Seismic Experiments and Data Processing

The seismic experiments presented here were conducted using the *S/V SHOYO* and *S/V TAKUYO* vessels in 2006 and 2007 under the Continental Shelf Surveys Project implemented by the Hydrographic and Oceanographic Department, Japan Coast Guard. We focused on two survey lines, MTr6 and MTr8 northwest of Minami-Tori Shima Island (Fig. 1). MTr6 and MTr8 run perpendicular and parallel to the paleomagnetic lineation, respectively. MTr6 intersects MTr8 perpendicularly 40 km from the northwestern end of MTr6. Since many small seamounts reflecting significant past igneous events are scattered in the eastern part of MTr6, we do not discuss this area in this paper.

For a controlled seismic source for wide-angle seismic experiments, we used an array of four air guns with a total volume of 96 ℓ (6,000 in^3) firing at intervals of 200 m. One hundred OBSs were installed at every 6 km along MTr6 and 17 OBSs were installed at every 10 km along MTr8. The positions of the OBSs were determined with the global search method (Oshida *et al*., 2008). Single-channel seismic reflection (SCS) data were also collected along the survey lines to estimate the thickness of the sediment layer. A non-tuned air gun array with a total capacity of 11 ℓ (700 in^3) firing at intervals of 50 m was used as a controlled source for SCS data.

The P-wave velocity structures were obtained through

doi:10.5047/eps.2010.02.011

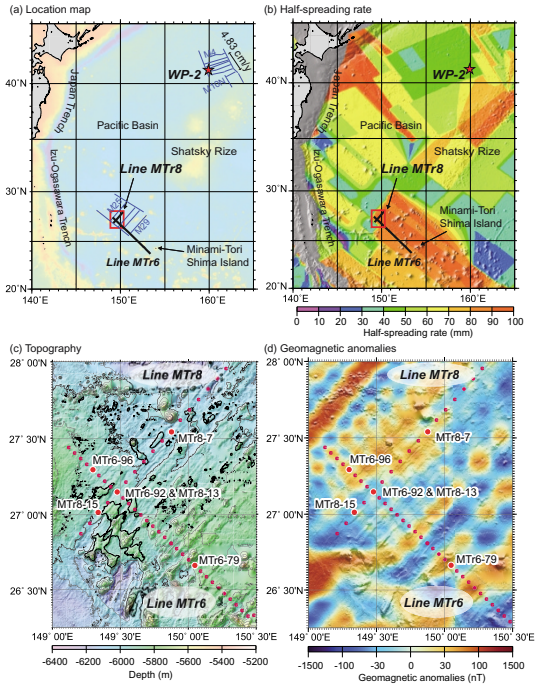

Fig. 1. (a) Location map of area explored in this study. Locations of our wide-angle seismic experiments are shown in black lines. Area located in the red rectangle is the target area for this study and is magnified in (c) and (d). The red star indicates the location of the seafloor borehole broadband seismometer (WP-2) employed by Shinohara *et al.* (2008). (b) Map showing half-spreading rates (Müller *et al.*, 2008) in the Northwest Pacific Basin. The rate in the studied area exceeds 80 mm/yr. (c) OBS deployment map with topography data. Red circles indicate positions of OBSs. Larger ones (MTr6-79, MTr6-96, MTr8-7, and MTr8-15) are the OBSs whose record sections are shown in Fig. 2. MTr6-92/MTr8-13 is the same OBSs deployed at the intersection of two survey lines. (d) Paleomagnetic map around the survey area. Two survey lines are set perpendicular and parallel to the paleomagnetic lineation.

the method reported in Kasahara *et al.* (2007) and Nishizawa *et al.* (2007, 2009). At first, we introduced the sedimentary layer thickness constrained by the SCS data. Then, we used the tomographic inversion method "tomo2d" coded by Korenaga *et al.* (2000) and forward modeling with trial and error using 2-D ray tracing (Fujie *et al.*, 2000; Kubota *et al.*, 2005). The first arrivals from the crust (P_c) and the uppermost mantle (P_n) were used in the tomographic inversion analysis. The size of the horizontal grid interval in the inversion is 0.5 km, and the vertical spacing gradually increases with the depth following the relationship $0.05 + (0.01 * \text{depth (km)})^{1/2}$ km. The velocity distribution inside the lower crust is derived mainly from later refraction arrivals propagating through the lower crust (P_g) and from reflection phases from the Moho (P_mP). The depth of the Moho was confirmed by the travel times of P_mP. The P-wave velocity of the uppermost mantle was determined from the P_n travel times.

We performed checkerboard resolution tests for the velocity models in order to obtain the resolution. The results show high reproducibility of the checkerboard pattern down to about 15 km in depth. In addition, we also modeled the amplitude data by calculating two-dimensional synthetic seismograms using the finite difference method E3D (Larsen and Schultz, 1995).

3. Results

3.1 Record sections and crustal structure of MTr6

The record sections of MTr6-79 and MTr6-96 (Fig. 2(a, b)) are of superior quality, and first arrivals can be observed even over a 100 km offset. Various phases of P-waves, such as P_c, P_g, P_mP, and P_n, are clearly recognized. The P-wave velocity structure of MTr6, which is shown in Fig. 3(a), was obtained from the travel times of these phases. The sedimentary layer of the structure model has a $V_p = 1.6$–2.5 km/s and is thinner than 0.5 km. The P-wave velocities in the upper crust are in the range 2.5–6.8 km/s and have a large velocity gradient of 2.0–3.3 km/s/km. The V_p of the lower crust is 6.8–7.1 km/s, with a small velocity gradient of 0.03–0.04 km/s/km. The boundary between the upper and the lower crust was modeled as a discontinuity in the velocity gradient. The total thickness of the crust is about 6.2–7.3 km, and the crustal structure is nearly homogeneous in the horizontal direction.

The P_n apparent velocities are considerably high, ranging between 8.4 and 8.9 km/s, as shown in Fig. 2(a, b). At first, we assumed that the P_n velocity is 8.4–8.9 km/s just below the Moho, whose depth was well constrained by a number of clear P_mP arrivals. However, the calculated P_n travel times were shorter than the ones observed in this model, and the offsets of 30–40 km where the P_n appears as a first arrival on the observed record sections are smaller than those in the observed data. Consequently, we carried out tomographic inversions for two initial models in which the crustal velocity structure down to the Moho is fixed and the uppermost mantle velocity is constant at 8.0 km/s and 8.6 km/s, respectively. The results for both models showed that the P-wave velocity distribution in the uppermost mantle is heterogeneous in both the horizontal and vertical directions and has slower areas at offsets of 70–90 km and 130–165 km within 5 km below the Moho.

Finally, we introduced these heterogeneous structures in the uppermost mantle into the velocity model and conducted forward modeling to confirm the propriety of the

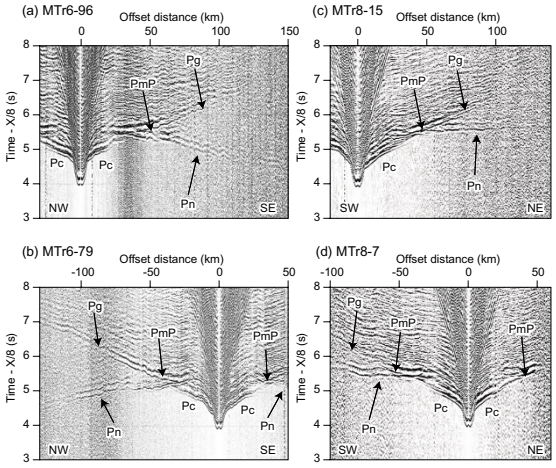

Fig. 2. Record sections of vertical-component seismograms (a: MTr6-96, b: MTr6-79, c: MTr8-15, d: MTr8-7). Vertical axis represents travel time (s) with a reduction velocity of 8.0 km/s. Horizontal axis denotes the offset distance in km from the OBS. P_c is the phase refracted through the crust, P_n is the mantle refraction phase, P_g is the later phase refracted through the crust, and P_mP is the phase reflected at the Moho.

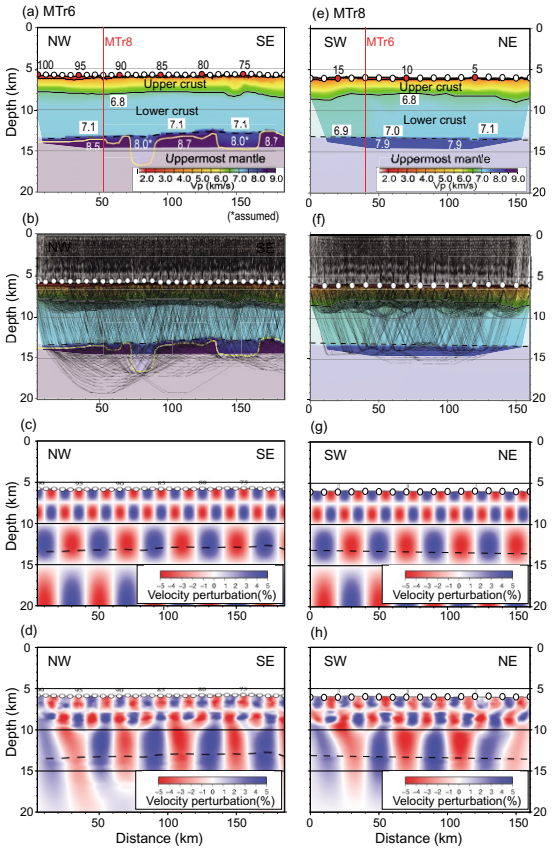

Fig. 3. *P*-wave velocity models and their reliability for MTr6 (a–d) and MTr8 (e–h). (a) *P*-wave velocity model for MTr6, where $V_p = 8.0$ km/s immediately below the uppermost mantle is an assumed value. (b) Ray diagrams for MTr6. (c) Initial pattern for the checkerboard test applied to MTr6 model. (d) Results of the checkerboard test for MTr6, and (e–h) results for MTr8. Black dashed lines indicate the Moho, and yellow lines in (a, b) represent the lower boundary limits of the heterogeneity. All checkerboard patterns down to a depth of 15 km are recovered, indicating that each constructed velocity model down to a depth of 15 km is reliable.

inversion results for constructing a final structural model. In the final model shown in Fig. 3(a, b), the value of V_p immediately below the Moho is 8.0 km/s through the profile and the depth at which $V_p = 8.5$–8.7 km/s fluctuates in the horizontal direction. The depths from the Moho to the areas where $V_p = 8.5$–8.7 km/s are 4 km at the offset of 70–90 km, 2 km at 130–165 km and about 0.7 km for the remaining regions. The velocity structures of the slower portions as inferred from the tomographic inversion cannot be constrained with high precision since their velocity and thickness are in a trade-off relationship. We estimated the velocity range for these areas as 8.0–8.5 km/s.

3.2 Record sections and crustal structure of MTr8

The record sections of MTr8-7 and MTr8-15 (Fig. 2(c, d)) show clear first arrivals up to an offset of approximately 100 km. A notable difference from the sections of MTr6 is the smaller P_n apparent velocity, which is in the range between 7.9 and 8.0 km/s.

The crustal velocity model for MTr8 is shown in Fig. 3(e, f). The V_p of the top sedimentary layer is 1.6–2.5 km/s, and the thickness is less than 0.5 km. The crust consists of an 1.6–2.5 km thick upper crust with $V_p = 2.5$–6.8 km/s and a 4.4–5.5 km lower crust with $V_p = 6.8$–7.1 km/s. The total thickness of the crust is about 6.8–7.4 km. These characteristics are almost the same as those for MTr6 (Fig. 3(a)), with the exception of the slightly lower velocity in the lower crust in the southwestern part of MTr8. The V_p in the uppermost mantle of MTr8 is 7.9 km/s, which is about 0.6–0.8 km/s lower than that for MTr6. Moreover, unlike MTr6, no heterogeneity was detected in the MTr8 uppermost mantle.

4. Discussion

4.1 Oceanic crust and uppermost mantle structure

The crustal velocity structures are almost the same for MTr6 and MTr8 in the Northwest Pacific Basin. The crust is composed of an upper crust with a high velocity gradient and a lower crust with a small velocity gradient. The total thickness of the crust is 6.2–7.4 km.

White *et al.* (1992) compiled a number of seismic profiles from previous studies conducted in the Pacific and Atlantic oceans. They reported that the average crustal structure composed of an upper crust with $V_p = 2.5$–6.6 km/s and a thickness of 2.11 ± 0.55 km and a lower crust with $V_p = 6.6$–7.6 km/s and a thickness of 4.97 ± 0.90 km. Our results are consistent with these characteristics. In addition, the total crustal thickness of 6.2–7.4 km as obtained in the 154–160 Ma area supports their suggestion that the crustal thickness appears to increase slightly with age, which is based on extremely few datasets from the older Pacific crust.

Recently, Shinohara *et al.* (2008) reported a crustal structure in the northern part of the Nortwest Pacific Basin (Fig. 1) on the basis of observations obtained through a seafloor borehole broadband seismometer. Their model also indicated a normal oceanic crust including a crust-mantle transition layer with a large velocity gradient, which was necessary to explain the observed large amplitudes of the P_n phases. We examined the presence of the Moho transition layer by calculating synthetic seismograms (Fig. 4) for models with a transition layer thickness ranging between 0.4 and 1.2 km using the E3D finite difference method (Larsen and Schultz, 1995). As the results obtained with

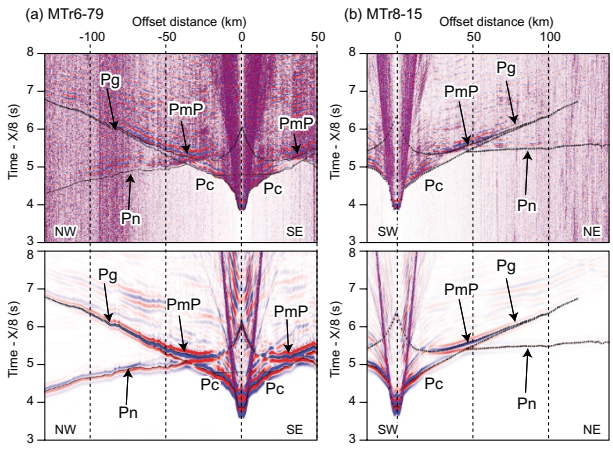

Fig. 4. Respective comparisons of observed record sections (top) and synthetic seismograms (bottom) for MTr6-79 (a: left) and for MTr8-15 (b: right). Calculated travel time curves for refraction arrivals from the crusts (P_c), from the uppermost mantle (P_n), and later phases through the crusts (P_g) are shown in the records together with reflection arrivals from the Moho ($P_m P$).

each model did not show significant discrepancies, we selected a simple model without a transition layer above the Moho shown in Fig. 3. The differences between our models and the model by Shinohara *et al.* (2008) suggest that the crust-mantle transition zone suggested by White *et al.* (1992) accounts for half of the normal ocean crustal structures in their dataset which exhibits first-order velocity discontinuities, with the other half displaying velocity gradients.

The uppermost mantle structure along MTr6 is characterized by a large heterogeneity immediately under the Moho. However, no clear relationships between the heterogeneity and the seafloor topography, the magnetic anomaly lineation, and the crustal structure were observed.

4.2 Velocity anisotropy in the uppermost mantle

The P_n velocity for MTr6 is around 8.5–8.7 km/s, which is significantly different from the value of 7.9 km/s obtained for MTr8, indicating the presence of velocity anisotropy of 7–10% in the uppermost mantle. MTr6 and MTr8 are nearly parallel and perpendicular to the magnetic lineation, respectively. In order to estimate the magnitude of anisotropy with high precision, additional survey lines running in different directions are necessary. Thus, the anisotropy of 7–10% as derived from only two lines in this study might be somewhat underestimated.

The result that the direction of higher velocity is perpendicular to the paleomagnetic lineation is consistent with anisotropy caused by the lattice preferred orientation of olivine crystals in the mantle when the oceanic plate was created at the mid-oceanic ridge (e.g., Hess, 1964; Raitt *et al.*, 1969). The velocity range (7.9–8.7 km/s) and the velocity anisotropy correspond to those of harzburgite, which is the predominant component of the upper mantle at fast-spreading ridges (Ismail and Mainprice, 1998).

Shinohara *et al.* (2008) also detected anisotropy in the uppermost mantle velocity in the Northwest Pacific Basin. They estimated the anisotropy at approximately 5%, which is smaller than our result of 7%. One of the possible reasons for this difference might be the dependence on the spreading rate. In this regard, Gaherty *et al.* (2004) showed that anisotropy observed in a slowly spreading area in the Atlantic Ocean with a half-spreading rate of 0.8–2.0 cm/yr has a small magnitude of 3.4±0.3%. The half-spreading rates of the areas in our study and those in the northeastern area as presented in Shinohara *et al.* (2008) are estimated to be >8 cm/yr (Müller *et al.*, 2008) and 4.83 cm/yr (Nakanishi *et al.*, 1992) from magnetic anomalies, respectively. Although our results support this relationship, more data is necessary in order to confirm it.

In this study, we performed a precise estimation of an unusually high velocity of more than 8.5 km/s and of large anisotropy in the uppermost mantle in the old and intact area of the Northwest Pacific Basin, which could provide important constraints for the evolution of the oceanic lithosphere at a high seafloor spreading rate.

Acknowledgments. The authors are grateful to Prof. Emeritus J. Kasahara, Dr. R. Kubota, Mr. K. Kokai, and the members of Japan Continental Shelf Surveys Co. Ltd. for performing data processing and analyses, as well as to Dr. S. Kodaira and Dr. Y. Ohara for their helpful comments. We also thank the captains and the crew of *S/V SHOYO* and *S/V TAKUYO*, Japan Coast Guard, as well as the members of the Hydrographic and Oceanographic Department, JCG, for managing the seismic surveys. Most of the figures in this paper were prepared using the GMT graphic package developed by Wessel and Smith. Finally, the authors thank K. Michibayashi and D. Lizarralde for their critical and constructive review of this work, which helped to greatly improve our manuscript.

References

Christensen, N. L. and M. H. Salisbury, Structure and composition of the lower oceanic crust, *Rev. Geophys.*, **13**, 57–86, 1975.

Fujie, G., J. Kasahara, T. Sato, and K. Mochizuki, Traveltime and raypath computation: A new method in a heterogeneous medium, *J. Soc. Explor. Geophys. Jpn.*, **53**, 1–11, 2000.

Gaherty, J. B., D. Lizarralde, J. Collins, G. Hirth, and S. Kim, Mantle deformation during slow seafloor spreading constrained by observations of seismic anisotropy in the western Atlantic, *Earth Planet. Sci. Lett.*, **228**, 255–265, 2004.

Hess, H. H., Seismic anisotropy of the uppermost mantle under oceans, *Nature*, **4945**, 629–631, 1964.

Ismail, W. B. and D. Mainprice, An olivine fabric database: an overview of upper mantle fabrics and seismic anisotropy, *Tectonophysics*, **196**, 145–157, 1998.

Kasahara, J., R. Kubota, T. Tanaka, S. Mizohata, E. Nishiyama, K. Tsuruga, Y. Tamura, A. Nishizawa, and K. Kaneda, A new integrated method for the crustal structure analysis using OBSs and control sources, *Eos Trans. AGU*, **88**(52), Fall Meet. Suppl., Abstract S12A-06, 2007.

Korenaga, J., W. S. Holbrook, G. M. Kent, P. B. Kelemen, R. S. Detrick, H.-C. Larsen, J. R. Hopper, and T. Dahl-Jensen, Crustal structure of the southeast Greenland margin from joint refraction and reflection seismic tomography, *J. Geophys. Res.*, **105**, 21591–21614, 10.1029/2000JB900188, 2000.

Kubota, R., E. Nishiyama, K. Murase, and J. Kasahara, Fast computation algorithm of ray-paths and their travel times including later arrivals for a multi-layered earth model, *Eos Trans. AGU*, **86**(52), Fall Meet. Suppl., Abstract S41A-0966, 2005.

Larsen, S. C. and C. A. Schultz, ELAS3D: 2D/3D elastic finite-difference wave propagation code, *LLNL internal report*, 18 p., 1995.

Müller, R. D., M. Sdrolias, C. Gaina, and W. R. Roest, Age, spreading rates and spreading symmetry of the world's ocean crust, *Geochem. Geophys. Geosyst.*, **9**, Q04006, doi:10.1029/2007GC001743, 2008.

Nakanishi, M., K. Tamaki, and K. Kobayashi, Mesozoic magnetic anomaly lineations and seafloor spreading history of the northwestern Pacific, *J. Geophys. Res.*, **94**, 15437–15426, 1989.

Nakanishi, M., K. Tamaki, and K. Kobayashi, Magnetic anomaly lineations from Late Jurassic to Early Cretaceous in the west-central Pacific Ocean, *Geophys. J. Int.*, **109**, 701–719, 1992.

Nishizawa, A., K. Kaneda, Y. Katagiri, and J. Kasahara, Variation in crustal structure along the Kyushu-Palau Ridge at 15–21°N on the Philippine Sea plate based on seismic refraction profiles, *Earth Planets Space*, **59**, e17–e20, 2007.

Nishizawa, A., K. Kaneda, N. Watanabe, and M. Oikawa, Seismic structure of the subducting seamounts on the trench axis: Erimo Seamount and Daiichi-Kashima Seamount, northern and southern ends of the Japan Trench, *Earth Planets Space*, **61**, e5–e8, 2009.

Oshida, A., R. Kubota, E. Nishiyama, J. Ando, J. Kasahara, A. Nishizawa, and K. Kaneda, A new method for determining OBS positions for crustal structure studies, using airgun shots and precise bathymetric data, *Explor. Geophys.*, **39**, 15–25, 2008.

Raitt, R. W., G. G. Shor Jr., T. J. G. Francis, and G. B. Morris, Anisotropy of the uppermantle, *J. Geophys. Res.*, **74**, 3095–3109, 1969.

Shinohara, M., T. Fukano, T. Kanazawa, E. Araki, K. Suyehiro, M. Mochizuki, K. Nakahigashi, T. Yamada, and K. Mochizuki, Upper mantle and crustal seismic structure beneath the Northwest Pacific Basin using a seafloor borehole broadband seismometer and ocean bottom seismometers, *Phys. Earth Planet. Inter.*, **170**, 95–106, 2008.

Shor, G. G., H. W. Menard, and R. S. Raitt, Structure of the Pacific Basin, in *The Sea*, vol. 4, Part 2, edited by A. E. Maxwell, pp. 3–27, Wiley-Interscience, New York, 1970.

White, R. S., D. M. Kenzie, and R. K. O'Nions, Oceanic crustal thickness from seismic measurements and rare earth element inversions, *J. Geophys. Res.*, **97**, 19,683–19,715, 1992.

M. Oikawa (e-mail: oikawa-m2nb@mlit.go.jp), K. Kaneda, and A. Nishizawa